
Improving Deep Generative Models on Many-To-One Image-to-Image Translation

Sagar Saxena

Department of Computer Science
University of Maryland
College Park, MD 20742
ssaxena1@umd.edu

Mohammad Nayeem Teli

Department of Computer Science
University of Maryland
College Park, MD 20742
nayeem@cs.umd.edu

Abstract

Deep generative models have been applied to multiple applications in image-to-image translation. Generative Adversarial Networks and Diffusion Models have presented impressive results, setting new state-of-the-art results on these tasks. Most methods have symmetric setups across the different domains in a dataset. These methods assume that all domains have either multiple modalities or only one modality. However, there are many datasets that have a many-to-one relationship between two domains. In this work, we first introduce a Colorized MNIST dataset and a Color-Recall score that can provide a simple benchmark for evaluating models on many-to-one translation. We then introduce a new asymmetric framework to improve existing deep generative models on many-to-one image-to-image translation. We apply this framework to StarGAN V2 and show that in both unsupervised and semi-supervised settings, the performance of this new model improves on many-to-one image-to-image translation.

1 Introduction

Many recent works in image-to-image translation have used deep generative models to learn state-of-the-art mappings between multiple domains. These models have been used for a wide array of tasks: colorization, style transfer, semantic image synthesis, image completion, super resolution, inpainting, and many more [33, 41, 28, 38, 2, 39]. Most approaches propose architectures that model this mapping as bijective [44, 17, 40, 24, 15, 25, 3], where each image from one domain can only map to one image in another domain, or many-to-many [13, 22, 4, 29], where each image from one domain can map to many in another domain. The ability to synthesize multiple images from one image is usually regarded as multi-modal image-to-image translation.

Many of the datasets that these methods are trained on, however, do not have bijective or many-to-many relationships between domains. In tasks such as image colorization [29], semantic segmentation [5, 9, 37, 14, 23], depth estimation [9, 26, 20], heat mapping [14], edge image synthesis [15, 44], etc., a model that learns either a bijective or many-to-many mapping between domains would not accurately model the relationship between domains. Instead of learning either uni-modal or multi-modal synthesis for all domains, a good model would learn uni-modal synthesis for domains that

only have one representation for each input image and multi-modal synthesis for domains that have multiple image representations for each input image.

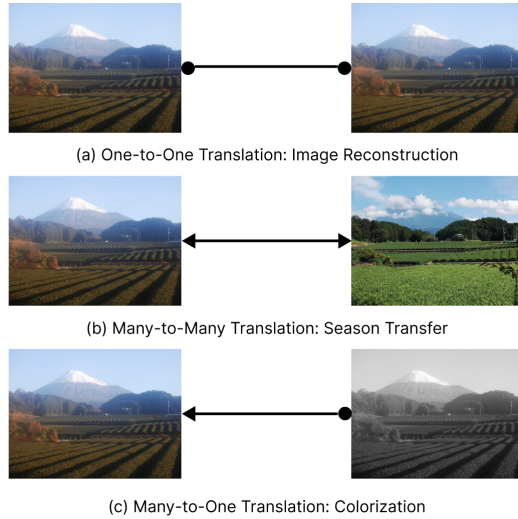


Figure 1: Different relationships between domains on [19]

To address this problem, we propose that if the domains have different types of modalities, the architecture of a model and its loss functions should also reflect this. In this paper, we discuss the development of deep generative image-to-image translation methods and why they may not be sufficient for datasets with many-to-one relationships between domains in Section 2. Our contributions include

- introducing a new framework that optimizes for many-to-one image translation and applying it to StarGAN V2 [4] in Section 3,
- providing a Colorized MNIST dataset and introducing a Color Recall metric that is more interpretable than existing metrics for ranking different architectures on many-to-one image translation tasks in Section 4,
- demonstrating, with experimental results, that the Colorized MNIST dataset can provide interpretable insights on a model’s ability to generate diverse images in Section 5.4,
- demonstrating, with experimental results on the Colorized MNIST and ADE20K [43, 42] datasets, that our method is able to either achieve better performance or a better trade-off when generating images in multiple domains with different modalities in Section 5

2 Related Work

2.1 Generative Adversarial Networks

Image-to-image translation with deep generative models has focused on Generative Adversarial Networks [8] (GANs). GANs generate realistic images by training a generator that generates images and an adversarial discriminator that discriminates whether images are real or fake. Initial work used paired data [15, 25] to create a bijective mapping between two domains by using a supervised loss function to ensure that each $x \in D_x$ mapped to a known $y \in D_y$.

To address the lack of paired data, the initial works were expanded to use unpaired data to learn bijective mappings [44, 17, 40, 24]. Two sets of generators and discriminators are trained in [44, 17, 40], with a cycle consistency loss to learn that each $x \in D_x$ maps to some $y \in D_y$ and back to the known $x \in D_x$. In [24, 3], there exists a shared latent space for all domains: for each unknown pair (x, y) there exists a shared z where z maps to $x \in D_x$ and $y \in D_y$.

More recent work uses unpaired data to learn many-to-many mappings. In [13, 22, 4], an additional style encoder is used to extract the styles from each domain and generators are modified to use both

the latent vector z and a style s . This style space can be either sampled or the style of a guide image can be extracted. By adding these style encoders, GANs were able to generate diverse outputs for a given input image across all domains. In [4], all weights are shared across domains and there is only one generator and discriminator for any number of domains. This increases scalability while reducing training time and model complexity.

Only a few works have attempted to leverage the many-to-one relationship between domains in a dataset [27, 34]. In [34], the discriminator was modified to produce an output map that labeled each pixel as either its class (for a semantic segmentation task) or "fake". While this approach produced state-of-the-art results on challenging semantic image synthesis tasks, it required paired inputs to train.

2.2 Diffusion Models

Recent work in diffusion models [11] has shown that diffusion models can outperform GANs in image synthesis [7]. The diffusion process gradually adds controlled noise to an image $x \in D_x$ to generate a latent $z \in \mathcal{N}(0, I)$. Diffusion models generate realistic images by training a parametrized Markov chain to reverse this diffusion process. Several approaches have emerged recently that take advantage of conditional diffusion models [1, 30] on image-to-image translation tasks.

In [29], the authors trained a diffusion model to create images $y \in D_y$ in the target domain and used the corresponding pair $x \in D_x$ from the source domain as an additional input during the diffusion process. Similar to initial works in GANs [15, 25], this model required paired examples and a supervised training paradigm.

Similar to [24, 3], a few approaches learn a shared latent space across domains [32, 35] to allow for unsupervised image-to-image translation. In [35], two diffusion models are used for each domain - one for mapping to a shared latent space and one for mapping from the shared latent space to the target domain.

Similar to [13, 4], [18] creates a disentangled latent space for content and style representations. [18] uses a complex approach that leverages vision transformers and contrastive and semantic style loss terms to generate high quality images. This indicates that, similar to GANs, new work in Diffusion Models will shift towards generating images from separate content and style latent spaces.

3 Optimizing For Many-To-One Image-To-Image Translation

The intuition for optimizing for many-to-one image-to-image translation is simple: if a dataset consists of domains that are asymmetric, model architecture should also be asymmetric. In both GANs and Diffusion Models, a few key loss terms and architectures are used to generate diverse and high fidelity images in all domains:

- shared weights with conditional inputs allow learning shared representations across domains,
- separating style and content spaces allows "diversity" to be embedded in the style space,
- crafted loss terms can help introduce higher diversity and desirable reconstructions.

We propose a few simple modifications when working with a many-to-one task:

- two domain-specific layers (one for decoding, one for encoding) should be used to map the original channel space to a shared channel space,
- for a uni-modal domain, only the content space should be used to generate the image,
- diversity should only be encouraged for multi-modal domains,
- optionally, when provided paired samples, a supervised loss should be assigned to the uni-modal domain.

3.1 Applying optimizations on StarGAN V2

StarGAN V2 is one of the best performing approaches for GAN-based image-to-image translation. In this section, we present how the modifications outlined above can be applied to StarGAN V2. The

base architecture for StarGAN V2 is slightly modified to use a Weight Demodulation layer instead of AdaIN [12] following [16].

StarGAN V2 consists of 4 modules: a style encoder E that creates a style vector s from an image x , a mapping network F that creates a style vector s from a latent vector $z \in \mathcal{N}(0, 1)$, a generator G that translates images given an input x and style s , and a discriminator D that outputs whether an image is real or fake given an image \hat{x} and domain d .

First, we add four channel mapping components $C_{A \rightarrow S}, C_{S \rightarrow A}, C_{B \rightarrow S}, C_{S \rightarrow B}$ that encode and decode from the original image channel space (in domains A and B) to a shared channel space (S). These are represented as trainable 1×1 convolutional layers. These networks are accompanied by simple cycle consistency loss terms:

$$L_{ch_cyc} = L1(C_{S \rightarrow A}(C_{A \rightarrow S}(x_A)), x_A) + L1(C_{S \rightarrow B}(C_{B \rightarrow S}(x_B)), x_B) \quad (1)$$

Ideally, we want to only use the content space to create images in the uni-modal domain (for simplicity let us assume that this is domain B) while maintaining the weight sharing between generators for both domains. In each weight demodulation component, the style vector s is inputted to a dense layer. The outputs of this dense layer scale the weights of the convolutional layer. Instead of directly modifying the components for the uni-modal domain, we can just use $s = 0$ for any uni-modal domain. This will have the effect of scaling the convolutional weights by the bias term of the dense layer (regardless of what E or F produces) and creating a fixed network for the unimodal domain. It will also zero any gradients that update the weights of the dense layer.

The original StarGAN V2 consists of a diversity synthesis loss term:

$$L_{ds} = -L1(G(x, s_1), G(x, s_2)), s_1 \neq s_2 \quad (2)$$

This loss term ensures that images that are generated with different styles are diverse. This, however, penalizes a model for correctly generating consistent images in a uni-modal domain. To address this, the diversity synthesis loss term can be rewritten as follows:

$$L_{ds} = -L1(G(x_B, s_1), G(x_B, s_2)), s_1 \neq s_2 \neq 0 \quad (3)$$

This ensures that we only penalize the model for diversity in the multi-modal domain. Throughout this paper, we will abbreviate this new model with the above modifications as HMU.

Given that we have pairs of images (x_A, x_B) , we can also add the following supervised loss term:

$$L_{sup} = L1(G(x_A, 0), x_B) \quad (4)$$

Throughout this paper, we will abbreviate the HMU model with this additional loss term as HMS.

4 Colorized MNIST Dataset

In this section, we introduce a Colorized MNIST dataset as a simple benchmark dataset for evaluating many-to-one image-to-image translation problems.

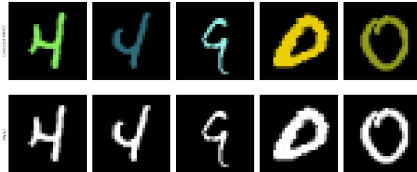


Figure 2: 5 paired samples from the Colorized MNIST dataset.

The MNIST [21] dataset consists of 60k training images and 10k test images of 10 digits. For each MNIST image, a random color is selected to generate a 3-channel colorized MNIST image.

$$x_a^{(i)} = c_i * x_b^{(i)}, x_b^{(i)} \in \text{MNIST}, c_i \in \mathbf{R}^3 \quad (5)$$

Models are trained to map between standard MNIST images and colored MNIST images (black/white \leftrightarrow color). Unlike other colorization tasks, this task is unique in that it can be composed of two independent tasks: first, regenerate the input image, then, sample a random color and paint the regenerated image. The color of the output image is independent of the input image.

This has the effect of cleanly dividing the latent space. The latent space for content representations should only encode the information needed to reproduce the MNIST image. The latent space for style representations should only encode the color space.

A good model should be able to generate MNIST images that have been painted with colors that are uniformly sampled. This color can be extracted by finding the pixel with the maximum intensity in a given image. We can measure how good a model is at sampling colors uniformly by creating an n-binned Color Recall score for each color channel.

Algorithm 1 Color Recall Score

Require: $n > 0$ ▷ Number of bins
Require: $c \in [\text{Red, Green, Blue}]$ ▷ Color channel
Require: D ▷ Dataset of real images
Require: \hat{D} ▷ Dataset of generated images
function BIN(p) ▷ The bin of a single pixel value
 return $\lfloor \frac{p * n}{n} \rfloor$
end function
function FREQ(D) ▷ Bin frequency in dataset D
 $F_c \leftarrow [0]$
 for all $x \in D$ **do**
 $p_c \leftarrow \max(x_c)$
 $b \leftarrow \text{bin}(p_c)$
 $F_c[b] \leftarrow F_c[b] + 1$ ▷
 end for
end function
 $F_c \leftarrow \text{freq}(D)$
 $\hat{F}_c \leftarrow \text{freq}(\hat{D})$
 $s \leftarrow \frac{1}{n} \sum_{b=0}^n \min(\frac{\hat{F}_c[b]}{F_c[b]}, 1)$ ▷ Average recall for each bin
return s

Another, simpler metric of interest is the number of unique colors that are in a generated dataset. Rather than having each pixel $p \in \mathbb{R}^3$, each pixel can be restricted to $p \in \mathbb{Z}^3 \cap [0, 255]$ (or 256 bins with a bin width of 1).

Algorithm 2 Unique Color Count

Require: D ▷ Dataset of images
 $S \leftarrow \emptyset$
for all $x \in D$ **do**
 $p_{rgb} \leftarrow \max(x)$ ▷ pixel with maximum intensity
 $S \leftarrow S \cup p_{rgb}$
end for
return $|S|$

Both of these metrics are easier to interpret than FID [10], Precision [31], and Recall [31], which rely on generating embeddings using a pre-trained neural network for real and generated images. Although this metric is tailored for the Colorized MNIST dataset, the goal of this section is not to present a new metric that works well on all datasets. Instead, this metric can be used in combination of the Colorized MNIST dataset to provide a more interpretable ranking and comparison of different models.

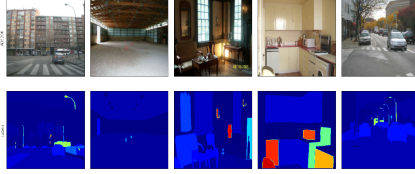


Figure 3: 5 samples from the ADE20K training set.

5 Experiments and Results

5.1 Datasets

We show results on 2 datasets: the Colorized MNIST dataset detailed in Section 4 and the more challenging ADE20K dataset [43, 42]. The ADE20K dataset contains 20k training and 2k test samples of RGB images of scenes and semantic segmentation maps of 150 different objects.

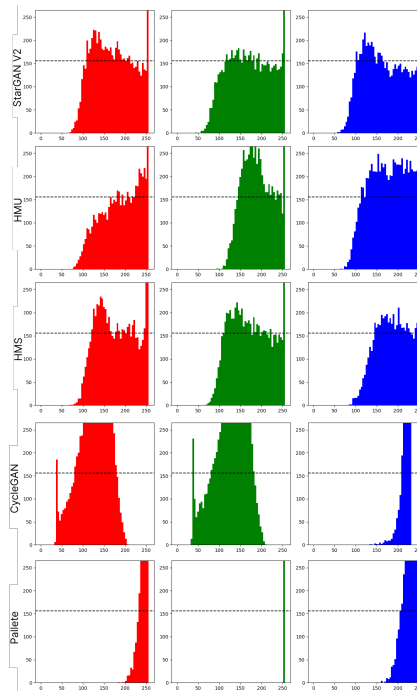


Figure 4: Red, Green, and Blue, Color Recall Histograms. The black dashed line represents the real uniform distribution of color values.

5.2 Metrics

Consistent with prior approaches, each model was evaluated on Fréchet Inception Distance [10] and Precision and Recall [31] with embeddings generated using the InceptionV3 [36] model. Precision and Recall curves are represented as a pair of two metrics, the F-8 and F-1/8 scores, as described in [31]. For the Colorized MNIST dataset, we include metrics on the Color Recall score and Mean Squared Error on the MNIST domain. For the ADE20K dataset, classification accuracy has also been reported. All metrics are reported on the test sets.

5.3 Training Details

All models were trained on 4 NVIDIA RTX A6000 GPUs on 100 thousand samples of image pairs (200k images total). Data samples were scaled between -1 and 1 during training. StarGAN V2 and all of its modifications were reimplemented to run with Python 3.9.6, TensorFlow 2.8, CUDA 11.3.1,

Model	Red	Green	Blue	Recall	Count
StarGAN V2	.6235	.6420	.6183	.6279	9374
HMU	.7037	.3843	.7126	.6002	9357
HMS	0.5774	0.6152	0.5204	0.571	8743
CycleGAN [44]	.5397	.5590	.1307	.4098	2474
Palette [29]	.1324	.0156	.2402	.1294	1096

Table 1: Color Recall Scores

Model	Colorized MNIST				MNIST			
	FID	F-8	F-1/8	C-Recall	FID	F-8	F-1/8	MSE
StarGAN V2	54.00	.5860	.7404	.6279	60.46	.4518	.7967	.1016
HMU	60.83	.4610	.5888	.6002	62.03	.2760	.4434	.0094
HMS	89.34	.3003	.5482	.5204	81.49	.3782	.6571	.0109

Table 2: Colorized MNIST \leftrightarrow MNIST Task Results

and cuDNN 8.2.1. All loss terms were weighted equally (with $\lambda = 1$). No additional modifications to the hyperparameters from the original StarGAN V2 paper (other than ones detailed in Section 3).

5.4 Colorized MNIST Results

In general, StarGAN V2, HMU and HMS were all able to successfully learn the mapping between colorized MNIST and MNIST images. Table 1 shows the results on the Color Recall score for the 3 color channels, an averaged total score, and the number of unique colors that were generated from the test set. Table 2 summarizes the results on FID, Precision, Recall, Mean Squared Error, and Color-Recall. Figure 5 shows visual results of image-to-image translation on 5 randomly sampled images from the test set.

In particular, the HMU model was able to outperform the base StarGAN V2 model with a lower MSE while only having a small decrease in color recall. The HMU model was also able to outperform StarGAN V2 on recreating red and blue and was able to capture a wider color range on those 2 channels.

Both the HMU and HMS models were able to improve on the original StarGAN V2 model by a factor of 10 on generating MNIST images. While the original model had marginally better FID, Precision, and Recall scores, the HMU model was able to achieve a better trade-off (a small loss in diversity in the multi-modal domain with a much larger improvement in mean squared error on the uni-modal domain). With the extra supervised loss term, the HMS model was able to achieve a near-similar performance on the mean squared error to the HMU model, but it also led to a larger loss in diversity. It’s possible that by reducing the supervised loss weight, the model would have improved performance.

To show the application of the Color Recall score, Table 2 also includes additional results on two popular architectures: CycleGAN [44], an unsupervised Generative Adversarial Network for image-to-image translation, and Palette [29], a supervised image-to-image translation conditional Diffusion Model. Although it is expected that CycleGAN performs poorly on the Color Recall score (it is known that CycleGAN is not able to produce diverse image distributions), Palette was proposed as a network that is able to produce images with high fidelity and diversity.

Figure 4 shows the distributions of the red, green, and blue values that were used to generate the scores. From this, it is simple to see that CycleGAN oversamples high-intensity blue values and Palette oversamples high-intensity green values. This indicates that CycleGAN colorizes MNIST images with different blue tints and Palette colorizes MNIST images with different green tints. Palette, in particular, oversamples high intensity values for all channels and captures a very small part of the color distributions.

5.5 ADE20K Results

As expected, the ADE20K dataset was significantly more challenging than the Colorized MNIST dataset. Table 3 summarizes the results on FID, Precision, Recall, Mean Squared Error, and Accuracy.

Model	Scenes			Labels				
	FID	F-8	F-1/8	FID	F-8	F-1/8	MSE	Accuracy
StarGAN V2	159.27	.1873	.1214	207.45	.0910	.0778	.4459	.0008
HMU	153.08	.2417	.2162	221.99	.0565	.0325	.3373	.0009
HMS	146.29	.3095	.2745	193.94	.1022	.0765	.2787	.0013

Table 3: ADE20K Scenes \leftrightarrow ADE20K Labels Task Results



Figure 5: 5 randomly sampled translations on the test set from Colorized-MNIST images to MNIST images (left) and MNIST images to Colorized MNIST images (right).

Figure 6 shows the visual results of image-to-image translation on 5 randomly sampled images from the test set.

The HMS model was able to outperform the baseline StarGAN V2 model on all metrics except for the F-1/8 score on the generated labels. The HMU model was also able to outperform the original model on all scene generation metrics. Notably, the MSE for the generated label maps decreases with the optimizations in HMU and further decreases with the supervised loss term in HMS. However, in all experiments, the label classification accuracy on the semantic segmentation task is low. This is expected as the model is not optimized for a semantic segmentation task. Label maps are represented as 2D maps with each pixel value corresponding to the class instead of 3D maps with one-hot vectors representing the classes and an L2 loss is used rather than a Categorical Cross Entropy loss.

Even with these additions, the StarGAN V2 generator architecture is not a good model to generate label maps. In Table 4, only the generator of the StarGAN V2 model is trained with an additional classification head that outputs logits for each class and penalized with a Sparse Categorical Cross Entropy loss. Results are included for 2 configurations: one configuration where the weights are initialized with the Xavier Uniform Initializer and one configuration where the weights of the HMS model are used to initialize the model. While using the HMS generator as pre-trained weights performs slightly better than without pretrained weights, the model is only able to achieve around a 7% accuracy in both configurations. This indicates that the StarGAN V2 generator is a poor model for generating label maps; choosing an alternative architecture that has been designed for a semantic segmentation task may help develop an improved generative network for both the scene generation and label classification tasks.

5.6 Limitations and Future Work

The approach outlined in Section 3 is limited to models that disentangle style and content space. This approach could extend to other methods, such as [34], that use noise vectors to introduce diversity

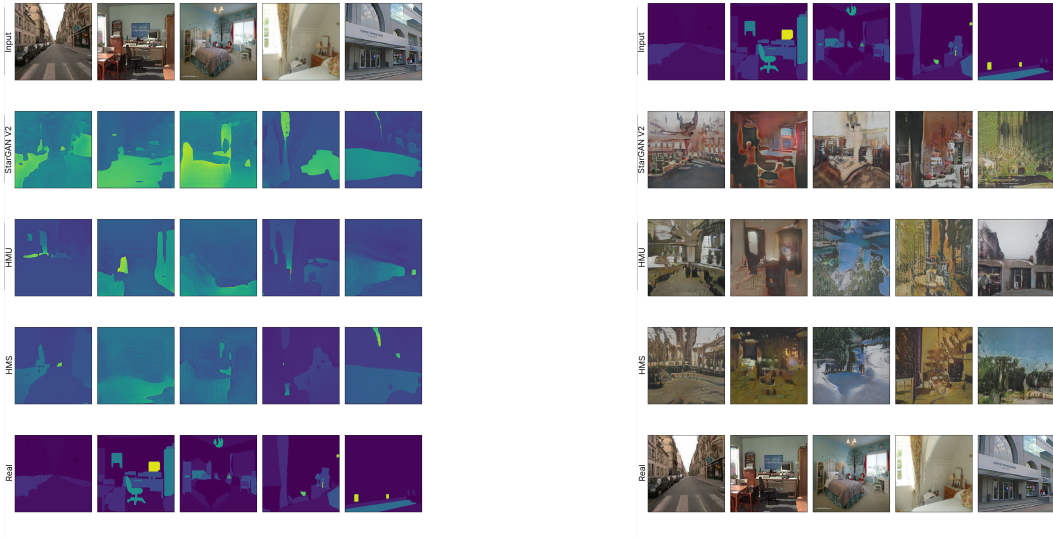


Figure 6: 5 randomly sampled translations on the test set from ADE20K scenes to ADE20K label maps (left) and ADE20K label maps to ADE20K scenes (right).

Pre-trained Weights	Accuracy
None	.0685
HMS	.0724

Table 4: Classification model accuracy on ADE20K dataset.

by setting the noise to 0 for uni-modal domains, but this has not been evaluated in this paper. The Color Recall results on Pallette, however, may indicate that disentangling content and style spaces is necessary to produce diverse image distributions.

All models did not perform well on the ADE20k dataset; however, the goal of this paper was not to introduce a new state-of-the-art technique for generating ADE20k images, but instead to propose a general approach to improving any generative model on many-to-one datasets.

Future work should expand this work by using better base model architectures (instead of StarGAN V2) to achieve state-of-the-art performance on more complex benchmark datasets [43, 42, 26, 9, 6]. Although the focus of this paper was not on pre-training, a promising application of many-to-one generative models could be to pre-train classification (i.e. semantic segmentation) or regression (i.e. depth estimation) models on tasks with limited labeled data. In many-to-one translation tasks, it can be less expensive to collect data for one domain than in another. Using the unsupervised HMU approach, it would be possible to pretrain with imbalanced datasets (for example, many real images and very few LiDAR images for depth estimation) and then fine-tune the weights for these tasks.

6 Conclusion

In this work, we have introduced a new framework to optimize generative image-to-image translation models for many-to-one tasks. We have shown that by applying this framework to StarGAN V2, we are able to achieve an improved joint performance on both the multi-modal and uni-modal domains. We have also introduced a new benchmark dataset and associated metrics that can be used to provide interpretable results on the ability of a model to perform many-to-one tasks.

References

- [1] Nanxin Chen, Yu Zhang, Heiga Zen, Ron J. Weiss, Mohammad Norouzi, and William Chan. Wavegrad: Estimating gradients for waveform generation. In *ICLR*, 2021.

- [2] Yuan Chen, Yang Zhao, Wei Jia, Li Cao, and Xiaoping Liu. Adversarial-learning-based image-to-image transformation: A survey. *Neurocomputing*, 411:468–486, 2020.
- [3] Yunjey Choi, Minje Choi, Munyoung Kim, Jung-Woo Ha, Sunghun Kim, and Jaegul Choo. Stargan: Unified generative adversarial networks for multi-domain image-to-image translation. In *Proceedings of the IEEE Conference on Computer Vision and Pattern Recognition*, 2018.
- [4] Yunjey Choi, Youngjung Uh, Jaejun Yoo, and Jung-Woo Ha. Stargan v2: Diverse image synthesis for multiple domains. In *CVPR*, pages 8185–8194, 06 2020.
- [5] Marius Cordts, Mohamed Omran, Sebastian Ramos, Timo Rehfeld, Markus Enzweiler, Rodrigo Benenson, Uwe Franke, Stefan Roth, and Bernt Schiele. The cityscapes dataset for semantic urban scene understanding. In *Proceedings of the IEEE Conference on Computer Vision and Pattern Recognition (CVPR)*, June 2016.
- [6] Jia Deng, Wei Dong, Richard Socher, Li-Jia Li, Kai Li, and Li Fei-Fei. Imagenet: A large-scale hierarchical image database. In *2009 IEEE Conference on Computer Vision and Pattern Recognition*, pages 248–255, 2009.
- [7] Prafulla Dhariwal and Alexander Nichol. Diffusion models beat gans on image synthesis. In M. Ranzato, A. Beygelzimer, Y. Dauphin, P.S. Liang, and J. Wortman Vaughan, editors, *Advances in Neural Information Processing Systems*, volume 34, pages 8780–8794. Curran Associates, Inc., 2021.
- [8] Ian J. Goodfellow, Jean Pouget-Abadie, Mehdi Mirza, Bing Xu, David Warde-Farley, Sherjil Ozair, Aaron C. Courville, and Yoshua Bengio. Generative adversarial nets. In *NIPS*, 2014.
- [9] Daniel Hernandez-Juarez, Lukas Schneider, Antonio Espinosa, David Vazquez, Antonio M. Lopez, Uwe Franke, Marc Pollefeys, and Juan Carlos Moure. Slanted stixels: Representing san francisco’s steepest streets. In *British Machine Vision Conference (BMVC), 2017*, 2017.
- [10] Martin Heusel, Hubert Ramsauer, Thomas Unterthiner, Bernhard Nessler, and Sepp Hochreiter. Gans trained by a two time-scale update rule converge to a local nash equilibrium. In *Proceedings of the 31st International Conference on Neural Information Processing Systems*, page 6629–6640, 2017.
- [11] Jonathan Ho, Ajay Jain, and Pieter Abbeel. Denoising diffusion probabilistic models. In H. Larochelle, M. Ranzato, R. Hadsell, M.F. Balcan, and H. Lin, editors, *Advances in Neural Information Processing Systems*, volume 33, pages 6840–6851. Curran Associates, Inc., 2020.
- [12] Xun Huang and Serge Belongie. Arbitrary style transfer in real-time with adaptive instance normalization. In *2017 IEEE International Conference on Computer Vision (ICCV)*, pages 1510–1519, 2017.
- [13] Xun Huang, Ming-Yu Liu, Serge J. Belongie, and Jan Kautz. Multimodal unsupervised image-to-image translation. In *ECCV*, 2018.
- [14] Soonmin Hwang, Jaesik Park, Namil Kim, Yukyung Choi, and In So Kweon. Multispectral pedestrian detection: Benchmark dataset and baseline. In *2015 IEEE Conference on Computer Vision and Pattern Recognition (CVPR)*, pages 1037–1045, 2015.
- [15] Phillip Isola, Jun-Yan Zhu, Tinghui Zhou, and Alexei A. Efros. Image-to-image translation with conditional adversarial networks. In *Proceedings of the IEEE Conference on Computer Vision and Pattern Recognition (CVPR)*, July 2017.
- [16] Tero Karras, Samuli Laine, Miika Aittala, Janne Hellsten, Jaakko Lehtinen, and Timo Aila. Analyzing and improving the image quality of StyleGAN. In *Proc. CVPR*, 2020.
- [17] Taeksoo Kim, Moonsu Cha, Hyunsoo Kim, Jung Kwon Lee, and Jiwon Kim. Learning to discover cross-domain relations with generative adversarial networks. In *Proceedings of the 34th International Conference on Machine Learning - Volume 70, ICML’17*, page 1857–1865. JMLR.org, 2017.
- [18] Gihyun Kwon and Jong Chul Ye. Diffusion-based image translation using disentangled style and content representation, 2023.
- [19] Pierre-Yves Laffont, Zhile Ren, Xiaofeng Tao, Chao Qian, and James Hays. Transient attributes for high-level understanding and editing of outdoor scenes. *ACM Transactions on Graphics (proceedings of SIGGRAPH)*, 33(4), 2014.
- [20] Kevin Lai, Liefeng Bo, Xiaofeng Ren, and Dieter Fox. A large-scale hierarchical multi-view rgb-d object dataset. In *IEEE*, pages 1817–1824, 05 2011.
- [21] Yann Lecun, Leon Bottou, Y. Bengio, and Patrick Haffner. Gradient-based learning applied to document recognition. *Proceedings of the IEEE*, 86:2278 – 2324, 12 1998.
- [22] Hsin-Ying Lee, Hung-Yu Tseng, Jia-Bin Huang, Maneesh Kumar Singh, and Ming-Hsuan Yang. Diverse image-to-image translation via disentangled representations. In *European Conference on Computer Vision*, 2018.
- [23] Tsung-Yi Lin, Michael Maire, Serge Belongie, James Hays, Pietro Perona, Deva Ramanan, Piotr Dollár, and C. Lawrence Zitnick. Microsoft coco: Common objects in context. In David Fleet, Tomas Pajdla, Bernt Schiele, and Tinne Tuytelaars, editors, *Computer Vision – ECCV 2014*, pages 740–755, Cham, 2014. Springer International Publishing.
- [24] Ming-Yu Liu, Thomas Breuel, and Jan Kautz. Unsupervised image-to-image translation networks. In I. Guyon, U. Von Luxburg, S. Bengio, H. Wallach, R. Fergus, S. Vishwanathan, and R. Garnett, editors, *Advances in Neural Information Processing Systems*, volume 30. Curran Associates, Inc., 2017.
- [25] Ming-Yu Liu and Oncl Tuzel. Coupled generative adversarial networks. In *Advances in Neural Information Processing Systems*, NIPS’16, page 469–477. Curran Associates Inc., 2016.
- [26] Pushmeet Kohli Nathan Silberman, Derek Hoiem and Rob Fergus. Indoor segmentation and support inference from rgb-d images. In *ECCV*, 2012.
- [27] Taesung Park, Ming-Yu Liu, Ting-Chun Wang, and Jun-Yan Zhu. Semantic image synthesis with spatially-adaptive normalization. In *Proceedings of the IEEE Conference on Computer Vision and Pattern Recogni-*

- tion, 2019.
- [28] P. Pradhyumna and Mohana. A survey of modern deep learning based generative adversarial networks (gans). In *2022 6th International Conference on Computing Methodologies and Communication (ICCMC)*, pages 1146–1152, 2022.
 - [29] Chitwan Saharia, William Chan, Huiwen Chang, Chris Lee, Jonathan Ho, Tim Salimans, David Fleet, and Mohammad Norouzi. Palette: Image-to-image diffusion models. In *ACM SIGGRAPH 2022 Conference Proceedings*, SIGGRAPH '22. Association for Computing Machinery, 2022.
 - [30] Chitwan Saharia, Jonathan Ho, William Chan, Tim Salimans, David J. Fleet, and Mohammad Norouzi. Image super-resolution via iterative refinement. *IEEE Transactions on Pattern Analysis and Machine Intelligence*, pages 1–14, 2022.
 - [31] Mehdi S. M. Sajjadi, Olivier Bachem, Mario Lučić, Olivier Bousquet, and Sylvain Gelly. Assessing Generative Models via Precision and Recall. In *Advances in Neural Information Processing Systems (NeurIPS)*, 2018.
 - [32] Hiroshi Sasaki, Chris G. Willcocks, and Toby P. Breckon. UNIT-DDPM: unpaired image translation with denoising diffusion probabilistic models. *CoRR*, abs/2104.05358, 2021.
 - [33] Sagar Saxena and Mohammad Nayeem Teli. Comparison and analysis of image-to-image generative adversarial networks: A survey. *CoRR*, abs/2112.12625, 2021.
 - [34] Edgar Schönfeld, Vadim Sushko, Dan Zhang, Jürgen Gall, Bernt Schiele, and Anna Khoreva. You only need adversarial supervision for semantic image synthesis. In *ICLR*, 09 2020.
 - [35] Xuan Su, Jiaming Song, Chenlin Meng, and Stefano Ermon. Dual diffusion implicit bridges for image-to-image translation. In *International Conference on Learning Representations (ICLR)*, May 2023.
 - [36] Christian Szegedy, Vincent Vanhoucke, Sergey Ioffe, Jonathon Shlens, and Zbigniew Wojna. Rethinking the inception architecture for computer vision. In *Proceedings of IEEE Conference on Computer Vision and Pattern Recognition*, 2016.
 - [37] Radim Tyleček and Radim Šára. Spatial pattern templates for recognition of objects with regular structure. In *Proc. GCPR*, Saarbrücken, Germany, 2013.
 - [38] Zhengwei Wang, Qi She, and Tomás E. Ward. Generative adversarial networks in computer vision: A survey and taxonomy. *ACM Comput. Surv.*, 54(2), feb 2021.
 - [39] Xian Wu, Kun Xu, and Peter Hall. A survey of image synthesis and editing with generative adversarial networks. *Tsinghua Science and Technology*, 22(6):660–674, 2017.
 - [40] Zili Yi, Hao Zhang, Ping Tan, and Minglun Gong. Dualgan: Unsupervised dual learning for image-to-image translation. In *2017 IEEE International Conference on Computer Vision (ICCV)*, pages 2868–2876, 2017.
 - [41] Ziqi Zhang, Zeyu Li, Kun Wei, Siduo Pan, and Cheng Deng. A survey on multimodal-guided visual content synthesis. *Neurocomputing*, 497:110–128, 2022.
 - [42] Bolei Zhou, Hang Zhao, Xavier Puig, Sanja Fidler, Adela Barriuso, and Antonio Torralba. Semantic understanding of scenes through the ade20k dataset. *arXiv preprint arXiv:1608.05442*, 2016.
 - [43] Bolei Zhou, Hang Zhao, Xavier Puig, Sanja Fidler, Adela Barriuso, and Antonio Torralba. Scene parsing through ade20k dataset. In *Proceedings of the IEEE Conference on Computer Vision and Pattern Recognition*, 2017.
 - [44] Jun-Yan Zhu, Taesung Park, Phillip Isola, and Alexei A Efros. Unpaired image-to-image translation using cycle-consistent adversarial networks. In *Computer Vision (ICCV), 2017 IEEE International Conference on*, 2017.